Mon. Not. R. Astron. Soc. **000**, 1–7 (2020) Printed 13 April 2020 (MN LATEX style file v2.2)

Eccentricity distribution of wide low-mass binaries

A. Tokovinin⋆
Cerro Tololo Inter-American Observatory/ NSF's National Optical-Infrared Astronomical Research Laboratory
Casilla 603, La Serena, Chile

-

ABSTRACT
Distribution of eccentricities of very wide (up to 10 kau) low-mass binaries in the solar neighborhood is studied using the catalog of El-Badry and Rix (2018) based on *Gaia*. Direction and speed of relative motions in wide pairs contain statistical information on the eccentricity distribution, otherwise inaccessible owing to very long orbital periods. It is found that the eccentricity distribution is close to the linear (thermal) one $f(e) = 2e$. However, pairs with projected separations <200 au have less eccentric orbits, while $f(e)$ for very wide pairs appears to be slightly super-thermal, with an excess of very eccentric orbits. Eccentricity of any wide binary can be constrained statistically using direction and speed of its motion. Thermal eccentricity distribution signals an important role of stellar dynamics in the formation of wide binaries, although disk-assisted capture also can produce such pairs with eccentric orbits.

Key words: binaries: visual

1 INTRODUCTION

Formation of binaries is an actively debated subject. It is already clear that multiple systems are formed by several different mechanisms and that binary statistics depend on the environment. However, quantitative and predictive models are still lacking.

Orbits of wide binaries are a fossil record of their formation process and early dynamical evolution. In this note, I focus on the eccentricity distribution. Dynamical interactions in a cluster produce a "thermal" eccentricity distribution $f(e) = 2e$. Dissipative forces (tides or gas friction) decrease the eccentricity. Ejections from unstable triples, on the contrary, produce wide binaries with very eccentric orbits and a "super-thermal" $f(e)$ (Reipurth & Mikkola 2012).

Here a catalog of wide binaries within 200 pc compiled by El-Badry & Rix (2018, hereafter ER2018) on the basis of *Gaia* second data release (Gaia collaboration 2018) is used. Accurate astrometry allows measurement of relative motion in the nearby resolved pairs, which, in turn, contains some information on the eccentricity. Tokovinin & Kiyaeva (2016) explored this option using classical (pre-*Gaia*) data on binaries within 67 pc with separations from 50 to a few hundred au. The new *Gaia* sample of wide binaries is larger and more accurate, allowing us to reach the regime of very wide separations.

The method of Tokovinin & Kiyaeva (2016) is based on the statistics of two quantities: (i) the angle γ between the line joining binary components and the direction of their orbital motion, and (ii) the normalized orbital speed μ'. The characteristic orbital speed μ^* (in angular units per year) is computed by the formula

$$\mu^* = (2\pi\rho)/P^* = 2\pi\rho^{-1/2}\varpi^{3/2}M^{1/2}, \qquad (1)$$

where ρ is the separation, P^* is the notional orbital period in years estimated for a face-on circular orbit from the projected separation $s = \rho/\varpi$, ϖ is the parallax, and M is the mass sum in solar units. If μ is the measured speed of the orbital motion, $\mu' = \mu/\mu^*$ is its normalized equivalent. A bound system must have $\mu' < \sqrt{2}$. The angle γ is folded in the $(0, 90^\circ)$ interval.

Simulations show that for a thermal eccentricity distribution, γ is distributed uniformly and uncorrelated with μ', while median $\mu' = 0.546$. If $f(e)$ is sub-thermal (i.e. the orbits are, on average, more circular), the median γ increases and becomes positively correlated with μ'. The fingerprint of a super-thermal distribution is just the opposite.

Relevant characteristics of nearby wide binaries and the role of inner subsystems are covered in Section 2. The eccentricity distribution is addressed in Section 3, first qualitatively by examining the distributions of μ' and γ, then by inverting these distributions to derive $f(e)$. Statistical constraints on the eccentricity of any given wide binary than can be deduced from its motion are outlined. Section 4 discusses the results in the context of binary formation.

⋆ E-mail: atokovinin@ctio.noao.edu

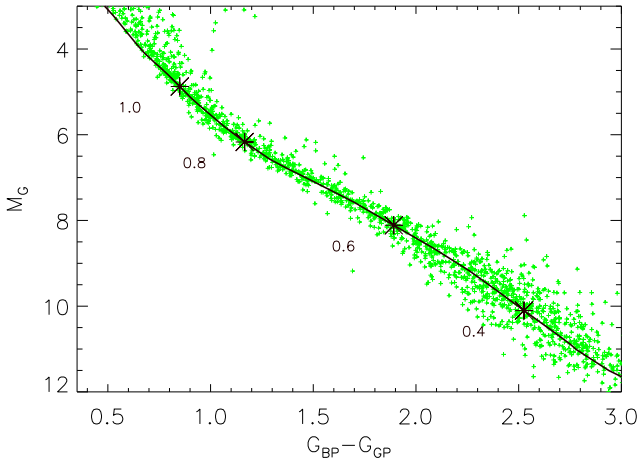

Figure 1. Color-magnitude diagram for primary (brighter) components of wide binaries within 67 pc. The dark line is a 1-Gyr solar-metallicity isochrone (Bressan et al. 2012) where the asterisks and numbers mark masses.

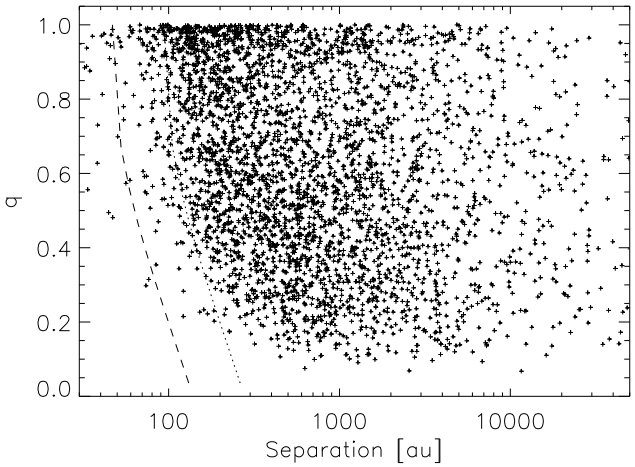

Figure 2. Correlation between separation and mass ratio. The dashed line is the *Gaia* detection limit at 67 pc, the dotted line is twice the limit.

2 CHARACTERISTICS OF THE SAMPLE

2.1 Catalog properties

The catalog of ER2018 was recovered from the journal web site as a comma-separated text file. Only 3601 pairs of main-sequence stars with both parallaxes exceeding 15 mas are kept in our subset of the catalog. The rationale for selecting only nearby pairs is the increased accuracy of the orbital speed measurement (particularly relevant for the widest pairs), better screening for subsystems, and access to low-mass, closer pairs. At larger distances, the ER2018 catalog suffers from increasing incompleteness.

Figure 1 shows the color-magnitude diagram (CMD) in the *Gaia* colors. The 1-Gyr PARSEC isochrone (Bressan et al. 2012) traces the main sequence. Masses are estimated from this isochrone and absolute G magnitudes. Some stars with masses above 1 $\mathcal{M}_\odot$ are evolved. To avoid evolved systems, the statistical analysis below is restricted to primary masses less than 1 $\mathcal{M}_\odot$, rejecting about 20% of the more massive pairs. Most pairs have primary components of G, K, M spectral types, with the lowest mass of about 0.2 $\mathcal{M}_\odot$ and the median mass of 0.6 $\mathcal{M}_\odot$. Figure 18 of El-Badry & Rix (2018) shows a binary-star sequence in the CMD which is practically absent in the sample studied here. The likely reason is better rejection of inner subsystems in nearby wide pairs.

Most pairs have separations between 100 and a few thousand au; the median separation is 460 au, corresponding to the orbital peiod of ∼10 kyr. The ER2018 catalog has a minimum angular separation of 2″ that translates to 133 au at 67 pc. Therefore, the number of pairs with $s < 133$ au is reduced substantially, preventing analysis of closer binaries. The maximum of the binary separation distribution at ∼50 au or less (Raghavan et al. 2010) is not sampled by this catalog. Consequently, I focus only on wide pairs.

Correlation between the mass ratio $q = M_2/M_1$ and separation is illustrated in Fig. 2: pairs with larger q tend to be closer and, conversely, wide pairs seem to prefer smaller q. Please, refer to El-Badry et al. (2019) for a more detailed study of the mass-ratio dependence on primary mass and separation. The dashed line is the approximate binary detection limit in *Gaia*, $\Delta G < 5.5(\rho-0.7)^{0.4}$ at maximum separation of 67 pc, converted into q by the relation $q \approx 1-0.16\Delta G$ valid for $M_1 \sim 0.6$ $\mathcal{M}_\odot$ (see Fig. 8 of El-Badry et al. 2019). The dotted line is the separation two times larger.

2.2 Multiple systems

The ER2018 catalog is not fully representative of the unbiased population of wide binaries for two main reasons. First, members of moving groups and clusters are excluded. Second, the selection method (good-quality astrometry and photometry, matching proper motions) creates a strong bias against subsystems. Remember that sub-arcsecond pairs often lack *Gaia* astrometry, hence have no chance to be present in the catalog as components of wider pairs. When *Gaia* does provide astrometry of both stars, it can still be distorted by subsystems (large errors and/or biased PMs), eliminating wide pairs containing subsystems from the catalog.

The ER2018 catalog was cross-identified with the 2018 version of the Washington Double Star (WDS) catalog (Mason et al. 2001) to look for known subsystems around primary and secondary components. The resulting list of 419 candidates was examined manually and compared to the Multiple Star Catalog, MSC (Tokovinin 2018), version of July 2019. Most hierarchies were already present in the MSC, the missing ones were added. It is well known that WDS contains optical and spurious pairs, and the cross-list counts many such cases. Decision on the reality of each subsystem, if not obvious, is based on the available data and my experience, and in some cases can be questioned. Overall, I found that 166 pairs in the ER2018 catalog within 67 pc contain known subsystems.

To further explore hidden multiplicity, I used the list of *Hipparcos* stars with astrometric accelerations by Brandt (2018) and matched stars within 67 pc with the WDS. Systems where the estimated period of the wide pair exceeds ∼1000 yr are triple. Several hundred new triples were added to the MSC as a result of this effort. After this update, comparison of MSC with the ER2018 catalog reveals 226 multiples, i.e. 60 additional hierarchies detected by acceler-

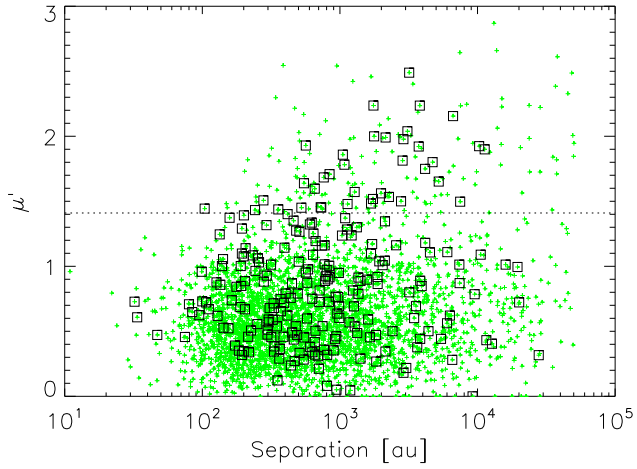

Figure 3. Statistics of "fast movers": dependence of μ' on projected separation. Known multiples are marked by squares, the dotted line marks $\mu' = 1.41$.

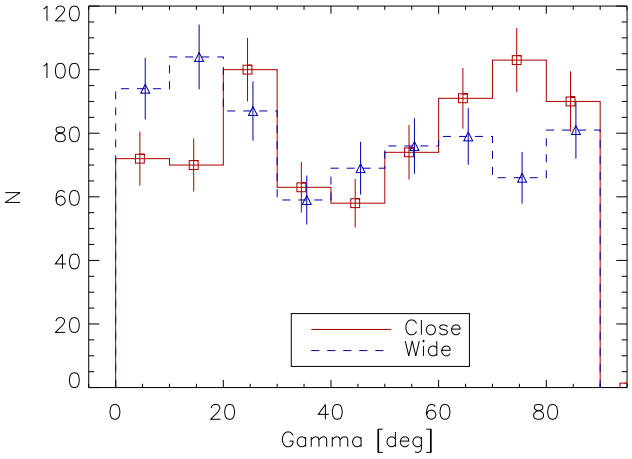

Figure 4. Histograms of γ for close ($100 < s < 250$ au, $N = 721$) and wide ($10^3 < s < 10^4$ au, $N = 715$) pairs.

ation. The total fraction of known multiples in the catalog is 0.063. In the following analysis, hierarchical systems (i.e. wide pairs with inner subsystems) present in the MSC are marked by a flag. Obviously, there remain many unknown subsystems, especially among fainter stars not covered by *Hipparcos* and Brandt (2018). El-Badry & Rix (2018) estimate that as much as 0.36 fraction of their sample could contain a subsystem in one or both components, despite the bias against multiples inherent to this catalog.

3 ECCENTRICITY DISTRIBUTION

3.1 Qualitative view

Parameters of the relative motion of wide pairs are computed from the *Gaia* astrometry provided in the ER2018 catalog. Modulus of the relative proper motion (PM) μ is computed from the PMs of each component, and its error is computed by eq. 6 in ER2018. The separation ρ and position angle θ of the pair are computed from the components' coordinates. The angle of the relative PM θ_μ is computed similarly. The angle γ is evaluated in three steps: $\gamma_1 = |\theta - \theta_\mu|$, $\gamma_2 = \gamma_1 \bmod 180^\circ$, $\gamma = \gamma_2$ for $\gamma_2 < 90^\circ$ and $\gamma = 90^\circ - \gamma_2$ otherwise. The error of γ is a relative PM error expressed in radians: $\sigma_\gamma = 57.3\ \sigma_\mu/\mu$, based on the assumption that PM errors are isotropic. The characteristic PM μ^* is computed using (1). The calculation of μ' accounts for a small bias due to measurement errors: $\mu' = \sqrt{\mu^2 - \sigma_\mu^2}/\mu^*$. However, the results are similar if this correction is neglected.

The following statistics uses wide pairs satisfying the following conditions:

- $M_1 < 1\ \mathcal{M}_\odot$
- $\sigma_\gamma < 50^\circ$
- $\mu' < 1.41$
- Not multiple

The large tolerance on σ_γ is intentional to avoid biases in the motions of wide pairs. Filtering leaves 2663 pairs for further analysis. Only 99 (3.7%) of the 2663 accepted pairs have $20^\circ < \sigma_\gamma < 50^\circ$, so a stricter cut on σ_γ could be adopted.

Apparently unbound pairs with $\mu' > 1.41$, or "fast movers", deserve a closer look. Their total number is 179, or 0.05 fraction of all pairs. Reasons such as measurement errors or hidden multiplicity reveal themselves in the statistics of fast movers explored in Fig. 3. Wide (hence slow) pairs should be more affected by these factors. Indeed, the fraction of fast movers increases with separation: it is 86/1086=0.079 for s between 10^3 and 10^4 au and 29/157=0.185 for $s > 10^4$ au. On the other hand, the fraction of fast movers does not depend on the distance. Therefore, measurement errors are not relevant and fast movers are mostly caused by inner subsystems. The fraction of known multiples among the fast movers, 37/179=0.21, is much larger than the fraction of multiples in the full catalog, 0.06.

Table 1. Medians of μ' and γ and correlation $C_{\mu'\gamma}$

Sample	N	$\gamma_{\rm med}$	$\mu'_{\rm med}$	$C_{\mu'\gamma}$
All	2663	44.7	0.542	−0.020
100–200 au	515	51.2	0.531	0.027
200–400 au	598	43.7	0.523	−0.09
$10^3 - 10^4$ au	715	41.5	0.554	0.012
Multiple	226	43.9	0.842	−0.057
$f(e) = 2e$	—	45.0	0.546	0.00
$f(e) = 1$	—	54.1	0.606	0.18
$e = 0$	—	68.3	0.677	0.61

Table 1 gives the median values of γ and μ' and their correlation coefficient $C_{\mu'\gamma}$ for the full sample and its subsets (close, wide, and multiple pairs). The last lines give theoretical parameters computed by Tokovinin & Kiyaeva (2016) by simulation of thermal and flat eccentricity distributions and for circular orbits. Multiples, excluded from the main sample, illustrate the influence of subsystems. They increase μ' by adding kinematic "noise" and bias the mass sum that affects μ^*. Indeed, multiples move faster than binaries (larger μ'). Subsystems should also randomize γ. Unrecognized multiples remaining in the sample influence the results to some extent, especially at large s.

Table 1 demonstrates that the global statistics of relative motion in wide pairs is perfectly compatible with the thermal eccentricity distribution. However, the sub-samples

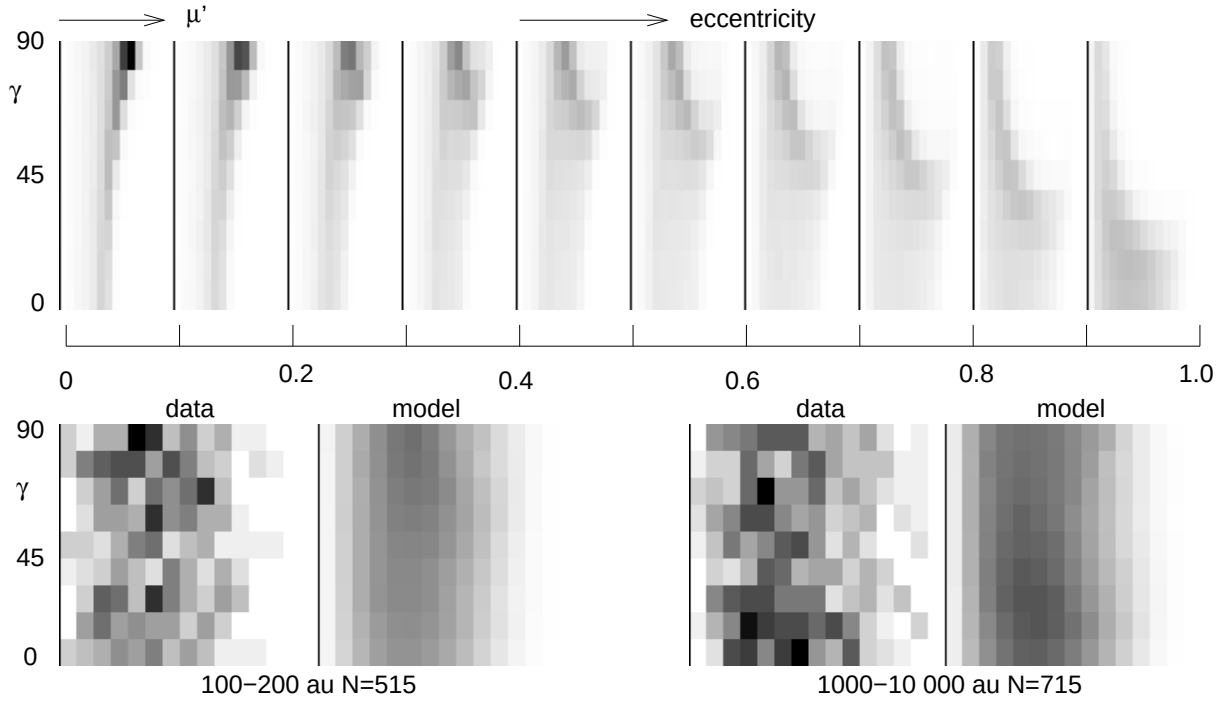

Figure 5. Restoration of the eccentricity distribution. Top row: ten templates in order of increasing eccentricity. Bottom row: observed histograms and their models.

of close and wider pairs deviate from the uniform distribution of γ in opposite ways. The difference between the medians, $9.6^\circ \pm 2.8^\circ$, is statistically significant. Figure 4 shows the distributions of γ for close and wide pairs. Close pairs are sub-thermal (less eccentric), wide pairs are super-thermal. Wide pairs seem to have an excess of $\gamma < 30^\circ$. Interestingly, the histogram for the close binaries might contain a similar excess, while the remaining pairs have a γ distribution increasing towards $\gamma = 90^\circ$, indicative of a sub-thermal eccentricity distribution.

When the sample is split into groups according to the mass ratio or primary mass, the resulting distributions of γ show no difference. However, when I compare 122 wide twins ($q > 0.95$) with $s > 500$ au with 213 similarly wide pairs with $0.8 < q < 0.95$, the median γ values are 36.7 ± 3.6 and 44.0 ± 3.9 degrees, respectively, suggesting that wide twins might have more eccentric orbits.

3.2 Recovering the eccentricity distribution

The eccentricity distribution $f(e)$ is derived using the method of Tokovinin & Kiyaeva (2016), briefly recalled here. The joint histogram of (μ', γ) is computed on a 15×9 grid (0.1 bin size in μ' and 10° bins in γ). Such distributions for simulated binaries with eccentricity in a narrow range, e.g. from 0 to 0.1, constitute a set of theoretical distributions (templates). Each template is evaluated for 10^4 simulated binaries. Parameters of simulated binaries such as mass sum, parallax, and separation are sampled randomly from the real data, and appropriate cuts are applied ($\rho > 2''$, $s > 100$ au, $\sigma_\gamma < 50^\circ$). This accounts for potential biases in the real sample.

The observed distribution of (μ', γ) is modeled by a linear combination of templates with 10 coefficients f_k satisfying the constraint $\sum_k f_k = 1$. Let $n_{i,j}$ be the number of binaries in the i-th and j-th bin of the histogram (i corresponds to μ' and j to γ), $T_{i,j,k}$ – the template for the k-th eccentricity bin, normalized to a unit sum over i and j. The model is $n'_{i,j} = N \sum_k T_{i,j,k} f_k$, where N is number of binaries. The goodness of fit is quantified by the parameter $\chi^2 = \sum_{i,j} (n_{i,j} - n'_{i,j})^2 / \sigma^2_{i,j}$, assuming Poisson errors $\sigma^2_{i,j} = n_{i,j}$ and $\sigma^2_{i,j} = 1$ if $n_{i,j} = 0$.

A small smoothing parameter α is introduced to favor continuous distributions and effectively damp the noise in the resulting f_k. The distribution f_k is found by minimizing

$$\sum_{i,j} (n_{i,j} - n'_{i,j})^2 + \alpha \sum_k (f_k - f_{k+1})^2 \rightarrow \min. \qquad (2)$$

with constraint $\sum_k f_k = 1$. A linear equation can be derived from (2), yielding the solution f_k as a simple matrix-vector product. Note that the minimization does not use weights corresponding to $\sigma_{i,j}$ for reasons explained by Tokovinin & Kiyaeva (2016), namely to reduce the influence of small $n_{i,j}$ that can be biased, e.g. by fast movers, and give more weight to the histogram bins with large values. Also, the regularization term is changed from $\alpha \sum_k f_k^2$ to the sum of squared differences. The new formulation models the data by a smooth distribution f_k, while the previous formulation biased the result towards a uniform distribution. However, the results of those two alternative regularization schemes are almost identical.

Adequacy of the model is confirmed by checking that the normalized values of $\chi^2/(135 - 9)$ are close to one (135 is the number of bins, 9 is the number of degrees of freedom). For 9 degrees of freedom, the "1 σ" confidence limit (68.3%) corresponds to the hyper-volume in the parameter space where χ^2 increases by less than 10.4 relative to its minimum (Press et al. 2007). The regularization parameter

Table 2. Eccentricity distribution

Separation	N	$\langle e \rangle$	$\chi^2/126$	f_1	f_2	f_3	f_4	f_5	f_6	f_7	f_8	f_9	f_{10}
100–10^4	2463	0.684	1.22	0.002	0.033	0.046	0.053	0.102	0.128	0.095	0.134	0.169	0.238
100–200	515	0.639	1.31	0.018	0.024	0.040	0.069	0.113	0.148	0.155	0.145	0.139	0.148
200–10^3	1233	0.677	1.25	0.000	0.033	0.049	0.059	0.092	0.124	0.119	0.140	0.171	0.213
10^3–10^4	715	0.683	1.37	0.023	0.029	0.040	0.059	0.080	0.096	0.113	0.147	0.188	0.227

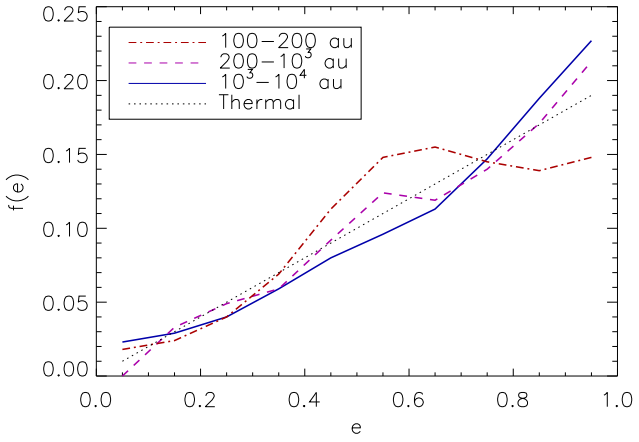

Figure 6. Eccentricity distributions.

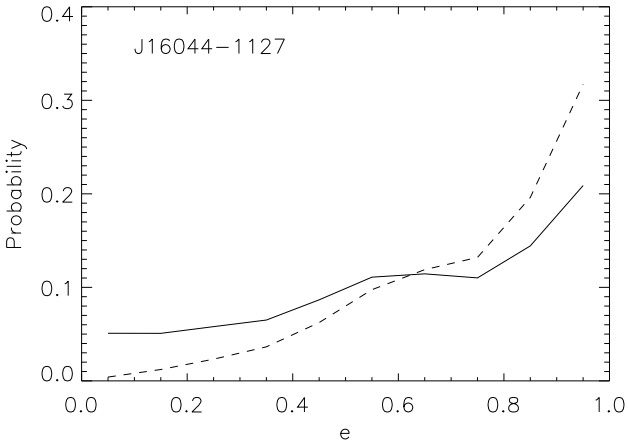

Figure 7. Posterior eccentricity distributions of ADS 9910 (WDS J16044−1127). Full line – uniform prior, dashed line – linear prior.

α is increased from 10^{-3} with a step of 2 times until the χ^2 exceeds its minimum value by more than 10.4; then the previous (one step back) α is adopted. Typically, $\alpha \approx 10^{-2}$ for $N \sim 500$.

The solution of (2) does not guarantee that all $f_k \geqslant 0$. When a negative f_k is encountered, it is set to zero and the fit is repeated with the reduced number of free parameters (so-called non-negative least squares).

Figure 5 illustrates the method. The upper panel shows 10 template distributions, all on the same gray scale. The vertical axis is γ, the horizontal axis is μ' ranging from 0 to 1.5 in each template. At small eccentricity, the maximum is near $\gamma = 90°$, $\mu' = 1$, while small γ dominate for eccentric orbits. The lower panels show the observed distributions in two separation ranges and their models.

The method was applied to the full sample and to various cuts in separation. Representative results are given in Table 2 and plotted in Fig. 6. The third column of Table 2 gives the mean eccentricity $\langle e \rangle$ and the goodness of fit metric $\chi^2/126$, which is larger than one because no weights are used. At intermediate separations, $f(e)$ is practically thermal. At separations below 200 au the deficit of large eccentricities becomes apparent, while at the largest separations $f(e)$ becomes slightly super-thermal. However, undetected subsystems mostly affect $f(e)$ at the largest separations, so the result should be taken with some caution.

At the shortest separations, the cuts applied to the data affect the statistics. The templates were re-computed by using only pairs with $s < 200$ au and, indeed, they differ from the templates obtained using the full sample, while looking qualitatively similar. For the small-separation sample, the calculation was repeated using those more appropriate templates. Indeed, a lower χ^2 was obtained, but the resulting $f(e)$ differs from the standard calculation by no more than 0.01.

3.3 Posterior eccentricity distribution

In some cases, constraints on the eccentricity of a particular wide binary are useful, e.g. to find minimum periastron separation and evaluate the influence of the wide companion on the inner subsystem or circumstellar disk. In response to this need, sampling techniques like "Orbits for the Impatient" (OFTI) were developed to derive posterior distributions of orbital parameters from incomplete data (Blunt et al. 2017). A simpler and faster way to relate the two observables $x_0 = (\mu', \gamma)$ with posterior eccentricity distribution is outlined here. The joint distribution of x and e can be written as

$$f(e, x) = f_1(x|e)\ f(e). \qquad (3)$$

If $f(e)$ in the right-hand part is replaced by the prior distribution $f_0(e)$ and x takes the observed value x_0, we obtain the posterior distribution $f(e|x_0)$. The conditional distribution $f_1(x|e)$ is obtained from simulations and is equivalent to the templates $T_{i,j,k}$ with suitable re-normalization.

To give an example, Fig. 7 plots posterior eccentricity distributions of a typical nearby wide binary ADS 9910 ($s =$ 335 au, $P^* = 4.5$ kyr) corresponding to the uniform and linear prior distributions $f_0(e)$. The observed parameters are $\mu' = 0.33$ and $\gamma = 30°$, there are no inner subsystems. Large eccentricity is more likely, but any eccentricity is possible, hence the constraint is fuzzy. However, in other instances the posterior constraints can be stronger and less dependent

on the prior. For example, for circular orbits $\mu' \leqslant 1$, so an observed value $\mu' > 1$ immediately excludes circular orbits. Similarly, large eccentricities can be ruled out for certain combinations of μ' and γ.

It is clear that the posterior distributions of orbital parameters such as eccentricity depend on the adopted prior distributions, i.e. are model-dependent. In the sampling methods like OFTI, the derived posterior distributions depend on the distribution of samples in the multi-dimensional space of orbital parameters. This work proves that a linear eccentricity distribution is the recommended prior for wide binaries, while a uniform prior should be deprecated in this context.

4 DISCUSSION

In § 5.1.4 of their review of multiplicity statistics, Duchêne & Kraus (2013) wrote that observations provide a "clear and uniform picture" of the eccentricity distribution, but in the same paragraph proposed two different models of $f(e)$, flat and Gaussian. Their discussion refers mostly to spectroscopic binaries. Figure 15 of Raghavan et al. (2010) gives $f(e)$ for visual binaries that is approximately flat between 0.1 and 0.6 and drops at large and small e. Based on this result, some authors adopted a flat $f(e)$ between 0 and 0.8 and $f(e) = 0$ at $e > 0.8$.

Tokovinin & Kiyaeva (2016) derived $f(e)$ than rises linearly at $e < 0.8$ and remains constant at larger e. The median separation in their sample was 120 au. This result is confirmed here using a different, larger sample (red curve in Fig. 6). They also show a good agreement with the $f(e)$ derived from known orbits with $P > 100$ yr, except the last bin lacking eccentric orbits. It is clear that the paucity of binaries with $e > 0.8$ in the sample of Raghavan et al. (2010) results from the bias in the orbit catalog and in fact such pairs are frequent.

At separations $s > 200$ au, the eccentricity distribution quickly evolves towards the thermal one. Moreover, this study shows that the widest pairs with $s > 1$ kau might have a slightly super-thermal eccentricity distribution. However, our results for the widest pairs are fragile, being affected by undiscovered subsystems. It is possible that the trend to super-thermal $f(e)$ at large separations is even stronger than found here.

A close match of the observed eccentricity distribution to the thermal distribution suggests that dynamical processes played an important role in the formation of wide binaries. For example, pairs that remain after dynamical interaction of a binary or a triple system with another star (scattering) have a nearly thermal $f(e)$ (e.g. Fig. 16 in Antognini & Thompson 2016). When two binaries interact dynamically in a gas cloud and survive as a 2+2 quadruple, the eccentricity of the wider remaining pair has a super-thermal distribution, while for the closer pair the distribution is thermal (Fig. 9 of Ryu et al. 2017). Wide binaries formed by ejection from unstable triples or "unfolding" (Reipurth & Mikkola 2012) must have only very eccentric orbits. However, the unfolding mechanism does not match certain properties of real wide binaries and appears to be exceptional rather than typical (Tokovinin 2017).

Hydrodynamical simulations show that protostars formed at large distances from each other can get bound into a wide pair with the help of gas friction (Bate 2019; Kuffmeier et al. 2019). Continued accretion onto such binary shortens its period and reduces the eccentricity. From this perspective, eccentric orbits are produced naturally even without dynamical interactions with other stars; a positive correlation between separation and eccentricity is expected. This formation channel of wide binaries works even in low-density environments. However, no predictions of the resulting eccentricity distribution are available so far. Simulations of a dense cluster by Bate (2019) inform on the binary statistics, but in this environment dynamical interactions between stars are important and the resultant statistics reflect a complex interplay of several processes.

To disentangle the relative roles of stellar dynamics and gas-assisted capture in the formation of wide binaries, it will be interesting to apply this method to sparse associations like Taurus-Auriga and to moving groups. Small sample size and account for the subsystems present obvious challenges.

ACKNOWLEDGMENTS

I thank Karim El-Badry and Maxwell Moe for comments on the early version of this work. This study used the Washington Double Star Catalog maintained at USNO. It has made use of data from the European Space Agency (ESA) mission *Gaia* (*https://www.cosmos.esa.int/gaia*), processed by the *Gaia* Data Processing and Analysis Consortium (DPAC, *https://www.cosmos.esa.int/web/gaia/dpac/consortium*). Funding for the DPAC has been provided by national institutions, in particular the institutions participating in the *Gaia* Multilateral Agreement.

REFERENCES

Antognini, J. M. O. & Thompson, T. A. 2016, MNRAS, 456, 4219
Bate, M. R. 2019, MNRAS, 484, 2341.
Blunt, S., Nielsen, E. L., De Rosa, R. J. et al. 2017, AJ, 153, 229
Brandt, T. D. 2018, ApJS, 239, 31
Bressan, A., Marigo, P., Girardi, L. et al. 2012, MNRAS, 427, 127
Duchêne, G. & Kraus, A. 2013, ARAA, 51, 269
El-Badry, K. & Rix, H.-W. 2018, MNRAS, 480, 488 (ER2018)
El-Badry, K., Rix, H.-W., Tian, H., et al. 2019, MNRAS, 489, 5822
Gaia Collaboration, Brown, A. G. A., Vallenari, A., Prusti, T. et al. 2018, A&A, 595A, 2 (Vizier Catalog I/345/gaia2).
Kuffmeier, M., Calcutt, H., & Kirstensen, L. E. 2019, A&A, 628, 112
Mason, B. D., Wycoff, G. L., Hartkopf, W. I., Douglass, G. G. & Worley, C. E. 2001, AJ, 122, 3466 (WDS)
Press, W. H., Teukolsky, S. A., Vetterling, T., & Flannery, B. P. Numerical Recipes, The Art of Scientific Computing. 2007, Cambridge Univ. Press, Cambridge
Raghavan, D., McAlister, H. A., Henry, T. J. et al. 2010, ApJS, 190, 1
Reipurth, B. & Mikkola, S. 2012, Nature, 492, 221

Ryu, T., Leigh, N. W. C., & Perna, R. 2017, MNRAS, 467, 4447
Tokovinin, A. & Kiyaeva, O. 2016, MNRAS, 456, 2070
Tokovinin, A. 2017, MNRAS, 468, 3461
Tokovinin, A. 2018, ApJS, 235, 6

5 SUPPLEMENTARY MATERIAL

The supplementary file lists μ, γ, μ^*, and other parameters described in the text for 3601 wide pairs from the ER2018 catalog located within 67 pc.